Combustion and Flame 187 (2018) 185–198

Contents lists available at ScienceDirect

Combustion and Flame

journal homepage: www.elsevier.com/locate/combustflame

Experimental and numerical study of the laminar burning velocity of CH_4–NH_3–air premixed flames

Ekenechukwu C. Okafor*, Yuji Naito, Sophie Colson, Akinori Ichikawa, Taku Kudo, Akihiro Hayakawa, Hideaki Kobayashi

Institute of Fluid Science, Tohoku University, 2-1-1 Katahira, Aoba-ku, Sendai 980-8577, Japan

ARTICLE INFO

Article history:
Received 24 March 2017
Revised 5 September 2017
Accepted 6 September 2017
Available online 3 October 2017

Keywords:
Methane
Ammonia
Laminar burning velocity
Reaction mechanisms
Markstein length

ABSTRACT

With the renewed interest in ammonia as a carbon-neutral fuel, mixtures of ammonia and methane are also being considered as fuel. In order to develop gas turbine combustors for the fuels, development of reaction mechanisms that accurately model the burning velocity and emissions from the flames is important. In this study, the laminar burning velocity of premixed methane–ammonia–air mixtures were studied experimentally and numerically over a wide range of equivalence ratios and ammonia concentrations. Ammonia concentration in the fuel, expressed in terms of the heat fraction of NH_3 in the fuel, was varied from 0 to 0.3 while the equivalence ratio was varied from 0.8 to 1.3. The experiments were conducted using a constant volume chamber, at 298 K and 0.10 MPa. The burning velocity decreased with an increase in ammonia concentration. The numerical results showed that the kinetic mechanism by Tian et al. largely underestimates the unstretched laminar burning velocity owing mainly to the dominance of $HCO\ (+H, OH, O_2) = CO\ (+H_2, H_2O, HO_2)$ over $HCO = CO + H$ in the conversion of HCO to CO. GRI Mech 3.0 predicts the burning velocity of the mixture closely however some reactions relevant to the burning velocity and NO reduction in methane–ammonia flames are missing in the mechanism. A detailed reaction mechanism was developed based on GRI Mech 3.0 and the mechanism by Tian et al. and validated with the experimental results. The temperature and species profiles computed with the present model agree with that of GRI Mech 3.0 for methane–air flames. On the other hand, the NO profile computed with the present model agrees with Tian et al.'s mechanism for methane–ammonia flames with high ammonia concentration. Furthermore, the burned gas Markstein length was measured and was found to increase with equivalence ratio and ammonia concentration.

1. Introduction

Interest in ammonia as a hydrogen carrier has recently been kindled in a search for safer and cheaper means of hydrogen transportation and storage. In comparison to the advanced materials for hydrogen storage such as metallic hydrides, ammonia has a relatively high hydrogen density, being made up of 17.8% by weight of hydrogen [1,2]. Ammonia, being one of the world's most produced chemicals, has a well-established production, transportation and storage infrastructure. Similar to hydrogen, ammonia is synthesised from fossil fuels and the CO_2 produced during the synthesis can be captured and sequestered [2]. On the other hand, ammonia can be produced from renewable CO_2 free energy sources [3]. Ammonia can be easily liquefied and stored at about 8.5 bar at room temperature or cooled to −33 °C and stored at ambient pressure. This makes its storage much less expensive than hydrogen storage, which requires about 350–700 bar for its storage at room temperature or −252.8 °C for its storage as a liquid at ambient pressure [4].

On the other hand, following the kindled interests in ammonia as a hydrogen carrier is a renewed interest in ammonia as a fuel. Ammonia is combustible and, being a carbon-free molecule, burns without carbon oxides emission. Ammonia is therefore considered a promising carbon-neutral fuel that offers great potentials of mitigating greenhouse gas emission. However, earlier applications and studies of ammonia as a fuel reported challenges associated with ammonia combustion [5,6]. Ammonia has a low burning velocity that is about five times lower than that of methane, a narrow flammable range, a high minimum ignition energy and a nitrogen atom in its molecule. These may result to low heat release rate, poor flame stabilisation characteristics, low combustion efficiency and high fuel NO emission etc. [6,7]. Nonetheless, our research team has recently demonstrated efficient application of ammonia for power generation in a micro gas turbine plant [8]. Other

* Corresponding author.
E-mail address: okafor@flame.ifs.tohoku.ac.jp (E.C. Okafor).

https://doi.org/10.1016/j.combustflame.2017.09.002
0010-2180/

means of employing ammonia as a fuel in internal combustion engines include the use of mixtures of ammonia and other fuels such as hydrogen [9–11], methane [12] and diesel [13,14].

Stabilisation of flames of ammonia containing mixtures on gas turbine combustors and the reduction of the high fuel NO emission from the flames are among the most important challenges in the development of gas turbine combustors for the fuels. Therefore, for the development of combustors for ammonia and blends of ammonia and other fuels, chemical kinetic mechanisms that accurately model the burning velocity of the mixtures and NO emissions from the flames are very relevant.

The laminar burning velocity is one of the most important properties of a mixture governing its combustion behaviour. It can serve as a parameter for characterising many premixed flame phenomena such as flashback, blow off or flame stabilisation on gas turbine combustors. It is also relevant in the validation and optimisation of reaction mechanisms. The laminar burning velocity is defined based on an adiabatic planar unstretched flame. However most practical laminar flame experience curvature and/or stretch, which results in the deviation of their burning velocities from those of the unstretched planar flames. Consequently, a method that correlates the stretched burning velocity with stretch and curvature needs to be used to extrapolate the laminar burning velocity of the stretched flame to that of an unstretched planar one [15].

The Markstein length, which is another important combustion property of a fuel, quantitatively expresses the sensitivity of the laminar burning velocity to flame stretch rate due to thermo-diffusive effects. It is an important parameter in the modelling of turbulent flames. Bradley et al. [16] concluded in their studies that the turbulent burning velocity may be affected by thermo-diffusive effects, hence may depend on the Markstein number i.e. the Markstein length normalised with the flame thickness. Although the Markstein number may correlate linearly with the Lewis number, which is easier to evaluate, the Markstein number is the preferred parameter to the Lewis number in turbulent flame modelling [17]. The Markstein length or the Markstein number is a more comprehensive expression of the phenomenon of response of a flame to stretch [18].

The present study focuses on measurement of the laminar burning velocity and development/optimisation of chemical kinetic mechanisms to accurately model the laminar burning velocity and NO emission from methane–ammonia mixtures. The fundamental combustion characteristics of methane have been well studied and numerous studies of methane flame chemistry have resulted to the development, optimisation and validation of kinetic mechanisms for modelling methane combustion, such as GRI Mech 3.0 [19], ARAMCO Mechanism v1.3 [20], University College San Diego Mechanism [21], etc. On the other hand, ammonia is an unconventional fuel, which has not been given much attention as a fuel for combustion applications. Therefore, even though several studies on ammonia oxidation chemistry have led to the development of ammonia oxidation mechanisms, there is limited data on some key combustion properties of ammonia mixtures for optimising and validating the mechanisms [7]. Hayakawa et al. [7] compared their measured unstretched laminar burning velocity of NH_3–air flames with numerical results obtained using the chemical kinetic mechanisms by Miller et al. [22], Lindstedt et al. [23], Konnov [24], Tian et al. [25], all of which were developed for ammonia combustion, and GRI Mech 3.0 [19]. They concluded that the mechanisms could not satisfactorily reproduce the measured burning velocity.

Similarly, there are limited experimental data on the laminar burning velocity of methane–ammonia flames. Most previous experimental studies on the fundamental combustion characteristics of methane–ammonia fuel concentrated mainly on the measurement of species profiles, being motivated by the need to understand and predict NO formation from the combustion of nitrogen-containing fuels. These studies provided important information on the structure of the flames and also resulted to the development of chemical kinetic mechanisms for the mixtures [24–29]. Tian et al. [25] developed a detailed reaction mechanism for methane–ammonia flames based on their experimental and numerical study of the structure of premixed $NH_3/CH_4/O_2$/Ar stoichiometric flames at 4 kPa using tuneable synchrotron vacuum ultraviolet photoionisation and molecular-beam mass spectrometry. The mechanism has a detailed methane and ammonia oxidation chemistry, consisting of 84 species and 703 elementary reactions. The study by Hayakawa et al. [7] showed that the laminar burning velocity of ammonia flames obtained using the mechanism by Tian et al. [25] was closer to the experimental result than were those obtained using the mechanisms by Miller et al. [22], Lindstedt et al. [23], and Konnov [24]. However, due to very limited experimental data on the laminar burning velocity of methane–ammonia flames, the available methane–ammonia reaction mechanisms, including Tian et al.'s [25], have not been validated or optimised for modelling the laminar burning velocity of the mixtures. So far, the only reported laminar burning velocity data on methane–ammonia flames are for trace quantities of ammonia in methane i.e. ammonia volume fractions less than or equal to 0.05 [26]. Furthermore, data on the Markstein length of methane–ammonia flames have not been reported so far.

In this study therefore, the unstretched laminar burning velocity of methane–ammonia–air flames were carefully measured for varying concentrations of ammonia in the binary fuel over a wide range of equivalence ratios. A detailed kinetic mechanism was developed to satisfactorily model the laminar burning velocity and NO concentration in the flames. Furthermore, the Markstein length of the mixtures was measured and its variation with equivalence ratio and ammonia concentration was investigated.

2. Experimental and numerical procedures

Figure 1 schematically shows the experimental setup used in this study. Experiments were carried out using a cylindrical constant volume combustion chamber. The inner diameter and length of the chamber were 270 mm and 410 mm, respectively. Two oppositely faced quartz glass windows of 60 mm in diameter allowed for optical access into the chamber. The combustible mixture quantities were prepared in the chamber according to the required partial pressures of the component gases using a GE UNIK 5000 silicon pressure sensor with an enhanced premium accuracy. The mixtures were ignited at a point along the central axis of the cylindrical chamber using capacitor discharge ignition (CDI). The diameter of the spark electrodes was 1.5 mm and the spark gap was set to 1 mm. The electrostatic energy, which was charged in the capacitor in the CDI circuit, was set to 0.3 J.

Flame propagation up to a diameter of 60 mm was observed and recorded by Schlieren photography via the quartz windows of the chamber with a high-speed digital camera (Photron, FASTCAM Mini UX100), while the pressure rise inside the chamber during flame propagation was measured using a Kistler pressure transducer. The pixel setting for the camera was 768 × 768 and the framing rates adopted ranged from 2500 to 6000 f/s, depending on the flame speeds. In addition, direct colour photographs were taken using the high-speed camera. The pixel resolution and frame rate of the colour imaging were 1024 × 1024 and 2500 f/s, respectively while the spatial resolution of the images was approximately 0.16 mm/pixel.

The studied conditions and properties of the mixtures are summarised in Table 1. The mixture temperature, T_u, and pressure, P_i, were 298 K and 0.10 MPa, respectively. Variations in the temperature of the mixtures were kept within ±3 K. As Fig. 2 shows, there was no pressure rise in the chamber during the period of record-

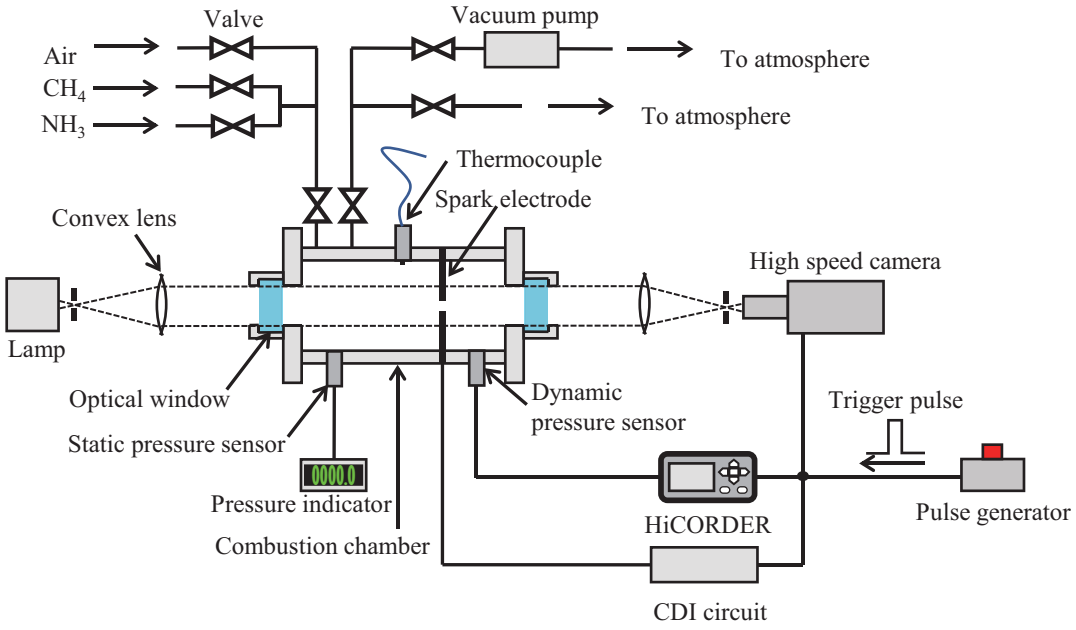

Fig. 1. Schematic diagram of the experimental setup.

Table 1
Properties of the mixtures in this study. The mixture temperature and pressure were 298 K and 0.10 MPa, respectively.

ϕ –	E_{NH_3} –	ρ_u kg/m^3	ρ_b kg/m^3	λ, W/m/K	c_p, J/kg/K	a, m^2/s	ν, m^2/s	Le –
	0	1.1243	0.1678	2.699×10^{-2}	1065	2.227×10^{-5}	1.584×10^{-5}	0.96
0.8	0.1	1.1193	0.1674	2.703×10^{-2}	1072	2.225×10^{-5}	1.583×10^{-5}	0.97
	0.2	1.1143	0.1671	2.707×10^{-2}	1079	2.222×10^{-5}	1.582×10^{-5}	0.97
	0.3	1.1095	0.1668	2.710×10^{-2}	1087	2.220×10^{-5}	1.581×10^{-5}	0.97
0.9	0	1.1198	0.1561	2.706×10^{-2}	1071	2.229×10^{-5}	1.585×10^{-5}	0.95
	0.1	1.1142	0.1557	2.710×10^{-2}	1079	2.226×10^{-5}	1.584×10^{-5}	0.97
	0.2	1.1088	0.1553	2.715×10^{-2}	1087	2.224×10^{-5}	1.583×10^{-5}	0.97
	0.3	1.1034	0.1550	2.719×10^{-2}	1096	2.221×10^{-5}	1.582×10^{-5}	–.97
1.0	0	1.1153	0.1483	2.714×10^{-2}	1077	2.231×10^{-5}	1.587×10^{-5}	–
	0.1	1.1093	0.1478	2.718×10^{-2}	1086	2.228×10^{-5}	1.586×10^{-5}	–
	0.2	1.1034	0.1473	2.722×10^{-2}	1095	2.225×10^{-5}	1.584×10^{-5}	–
	0.3	1.0976	0.1468	2.727×10^{-2}	1104	2.222×10^{-5}	1.583×10^{-5}	–
1.1	0	1.1109	0.1469	2.721×10^{-2}	1084	2.232×10^{-5}	1.588×10^{-5}	1.10
	0.1	1.1044	0.1465	2.725×10^{-2}	1093	2.229×10^{-5}	1.587×10^{-5}	1.10
	0.2	1.0981	0.1462	2.730×10^{-2}	1103	2.226×10^{-5}	1.586×10^{-5}	1.10
	0.3	1.0919	0.1458	2.735×10^{-2}	1113	2.223×10^{-5}	1.584×10^{-5}	1.10
1.2	0	1.1065	0.1488	2.728×10^{-2}	1090	2.234×10^{-5}	1.590×10^{-5}	1.10
	0.1	1.0996	0.1484	2.733×10^{-2}	1100	2.230×10^{-5}	1.588×10^{-5}	1.10
	0.2	1.0929	0.1481	2.737×10^{-2}	1111	2.227×10^{-5}	1.587×10^{-5}	1.10
	0.3	1.0863	0.1478	2.743×10^{-2}	1121	2.224×10^{-5}	1.586×10^{-5}	1.10
1.3	0	1.1023	0.1513	2.735×10^{-2}	1096	2.235×10^{-5}	1.591×10^{-5}	1.10
	0.1	1.0950	0.1509	2.740×10^{-2}	1107	2.232×10^{-5}	1.589×10^{-5}	1.10
	0.2	1.0878	0.1505	2.745×10^{-2}	1118	2.228×10^{-5}	1.588×10^{-5}	1.10
	0.3	1.0809	0.1501	2.750×10^{-2}	1130	2.224×10^{-5}	1.586×10^{-5}	1.10

ing of the flame images at all conditions. Hence, the measurements were considered to have been completed at the adopted mixture pressure and temperature. The equivalence ratio was varied from 0.8 to 1.3. The concentration of NH_3 was expressed in terms of the heat fraction of NH_3 in the binary fuel, E_{NH_3} as expressed in Eq. (1)

$$E_{NH_3} = \frac{x_{NH3}LHV_{NH3}}{x_{NH3}LHV_{NH3} + x_{CH4}LHV_{CH4}} \quad (1)$$

Here, x_{NH_3} and x_{CH_4} are mole fractions of NH_3 and CH_4 in the binary fuel while LHV stands for the lower heating value. The value of E_{NH_3} was varied from 0 to 0.3, corresponding to a variation in x_{NH_3} from 0 to 0.52. At least four experiments were done at each examined condition and the unstretched laminar burning velocity and burned gas Markstein length were obtained as the averaged value. The largest scatter in the measured unstretched laminar burning velocity was less than 5% of the average value while that for the Markstein length was less than 10% of the average value. On the other hand, the largest estimated uncertainty in the measured laminar burning velocity was about 12%. The major sources of uncertainty in the present study were mixture preparation and radiation effects. The uncertainty in obtaining the equivalence ratio of multicomponent fuel mixtures using the partial pressure method is larger than that of the single component fuels [15]. A GE UNIK 5000 silicon pressure sensor with an enhanced premium accuracy

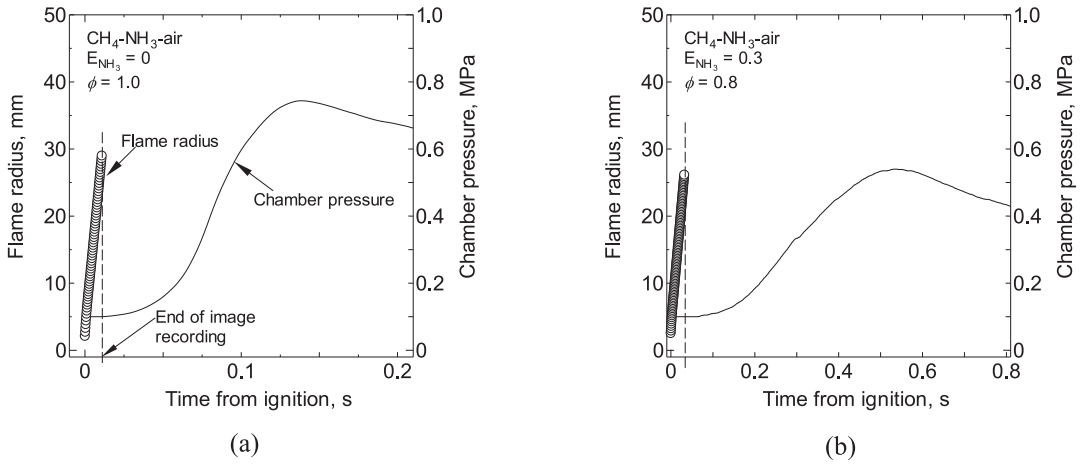

Fig. 2. Chamber pressure-time and radius-time histories of the relatively fast and relatively slow burning flames.

was used in this study to minimize the uncertainties in mixture preparation.

Chen [30] noted that other possible sources of uncertainty in laminar burning velocity measurements using outwardly propagating flames include confinement, flame instability, ignition energy, buoyancy, nonlinearity of flame speed-stretch rate relationship, etc. The effects of confinement were considered to be insignificant in this study because the inner diameter of the combustion chamber was sufficiently larger than the maximum recordable flame diameter. Hence, rise in chamber pressure during recording of flame propagation was avoided as shown in Fig. 2. In addition, the flames in the present study did not show any tendency to become unstable within the recorded range of flame radii, hence instability did not contribute to experimental uncertainty. Furthermore, the effect of ignition energy was considered to have been avoided in the reported results because flame radii larger than 10 mm were used in extracting the unstretched laminar burning velocity and the Markstein length as discussed later. Moreover, the suitability of the linear and the nonlinear stretch extrapolation methods were carefully considered to avoid uncertainties arising from nonlinearity of the flame speed-stretch rate relationship. On the effects of buoyancy, Ronney and Wachman [31] reported that the effect of buoyancy on the laminar burning velocity became noticeable for flames with laminar burning velocity less than 15 cm/s. Few of the flames in this study had unstretched laminar burning velocity slightly less than 15 cm/s. The effect of buoyancy on the burning velocity of these flames was considered insignificant since there was no noticeable change in the flame symmetry, neither did the flames drift upwards during propagation.

In addition to the experiments, one-dimensional adiabatic and unstretched laminar flames of the mixtures were simulated using ANSYS Chemkin-PRO [32]. The software was used in computing the unstretched laminar burning velocity, species concentration, rate of production of species and was also used for sensitivity analysis. The unstretched laminar burning velocity, s_l, was defined as the velocity at the cold boundary in the computational domain. Detailed combustion mechanisms such as GRI Mech 3.0 [19], and the mechanisms by Tian et al. [25], Mendiara et al. [29], and University College at San Diego [21] were employed in simulating the unstretched laminar burning velocity. For the purpose of the discussion in this paper, these mechanisms shall be referred to as GRI Mech 3.0, Tian Mech, Mendiara Mech, and UCS Mech respectively. A detailed chemical kinetic model based mainly on GRI Mech 3.0 [19] with important ammonia oxidation steps from Tian Mech [25] was developed in this study for modelling methane–ammonia flames. The developed kinetic model consists of 59 species and 356 elementary reactions

3. Evaluating the laminar burning velocity and Markstein length from the experiments

The radius of the spherical propagating laminar flames were measured with time from the recorded Schlieren images. Representative raw radius-time record of each flame in this study is provided in the supplementary material. The laminar flame speeds, s_n, were derived from the radius-time record of the flames according to Eq. (2);

$$s_n = \frac{dr_{sch}}{dt} \tag{2}$$

where r_{sch} is the radius of the flame obtained from the Schlieren images and t is time. Spherical propagating flames are affected by stretch due to curvature or aerodynamic strains. Hence, s_n, here referred to as the stretched laminar flame speed of the spherical flame, is dependent on the total flame stretch rate, ε. The total flame stretch rate of a propagating spherical flame is defined as the time rate of change of flame area per unit area as given below [33].

$$\varepsilon = \frac{1}{A_f}\frac{dA_f}{dt} = \frac{2}{r_{sch}}\frac{dr_{sch}}{dt} \tag{3}$$

where A_f is the area of the spherical flame front. Various correlations between s_n and ε have been proposed in literature which enable the elimination of the effect of stretch from the measured stretched flame speed by extrapolating s_n to zero stretch rate [15]. Consequently, the unstretched flame speed and the Markstein length with respect to the burned gas could be obtained from the measured results. Clavin [34], in their studies of the dynamics of premixed flame fronts governed by one-step irreversible chemical reaction with large activation energy, showed that the flame speed, s_n, of a weakly stretched flame may vary with flame stretch rate, ε, according Eq. (4).

$$s_s - s_n = L_b.\varepsilon \tag{4}$$

Here, s_s is the unstretched flame speed while L_b is the Markstein length with respect to the burned gas. This correlation has been used by numerous research groups for evaluating s_s and L_b. According to Eq. (4), the unstretched flame speed is derived as the intercept value of s_n at $\varepsilon = 0$ by linearly extrapolating the stretched flame speed to an infinite flame radius (or a stretch rate of zero).

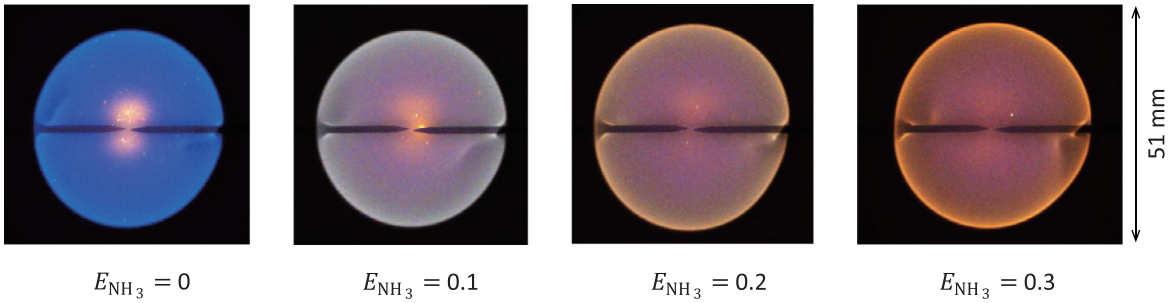

Fig. 3. Direct photograph images of the flames at a diameter of about 40 mm, showing the change in the chemiluminescence with change in ammonia concentration. The photographs were taken with the same camera setting.

The unstretched laminar burning velocity, s_l is then obtained by a mass balance across the unstretched flame, which results to $s_l = s_s/\sigma$. Here σ is the ratio of the unburnt mixture density, ρ_u, to the burnt gas density, ρ_b. The burned Markstein length is obtained as the negative slope of the linear graph [11,35–37].

Kelley and Law [38] observed that flames such as n-butane flames, with Lewis number sufficiently far from unity, may exhibit a non-linear s_n vs. ε relationship. Therefore they proposed the following non-linear correlation for extracting the unstretched flame speed and the burned Markstein length.

$$\left(\frac{S_n}{S_s}\right)^2 \ln\left(\frac{S_n}{S_s}\right)^2 = -2\frac{L_b\varepsilon}{S_s} \tag{5}$$

It can be shown from Eq. (5) that $\ln(s_n)$ varies linearly with $\varepsilon/{s_n}^2$, with an intercept on the $\ln(s_n)$ axis equal to $\ln(s_s)$ and a slope equal to $-s_sL_b$. Hence, s_s and L_b can be obtained from linear extrapolation of $\ln(s_n)$ vs. $\varepsilon/{s_n}^2$ plots [39].

It was concluded by Chen [39] and Wu et al. [40] that the accuracies of the different correlations in literature strongly depend on the Lewis number of the mixtures. Chen [39] noted that the linear correlation, Eq. (4) is suitable for mixtures with Lewis number close to unity while the non-linear correlations are more appropriate for mixtures with Lewis numbers far from unity because of the non-linear trend in their s_n vs. ε relationship. However, it was found in this study that the linear correlation may not always be appropriate for mixtures with Lewis numbers close to unity. In this study, the Lewis number of the binary fuel, defined simply as the mole-weighted Lewis numbers of the deficient reactants, was close to unity and did not vary significantly with ammonia concentration at all equivalence ratios as shown in Table 1. However, the linear correlation, Eq. (4), was found increasingly less accurate than the non-linear method, Eq. (5), for extracting the unstretched laminar burning velocity and the Markstein length as the equivalence ratio and ammonia concentration increased. This was due to increasing non-linearity of the flame speed-stretch rate relationship owing to the influence of an increase in the flame thickness as discussed in the following sections.

4. Results and discussion

4.1. Flame observation

Figure 3 shows images of the stoichiometric flames taken by direct colour photography. As shown, the colour of the flames gradually changed from blue, typical of hydrocarbon flames, to orange as the concentration of ammonia in the binary fuel varied from $E_{NH_3} = 0$ to 0.3. Hayakawa et al. [7] showed that pure ammonia flames have an orange chemiluminescence and concluded that the orange chemiluminescence was due to the $NH_2\alpha$ band and the super-heated H_2O vapour spectra.

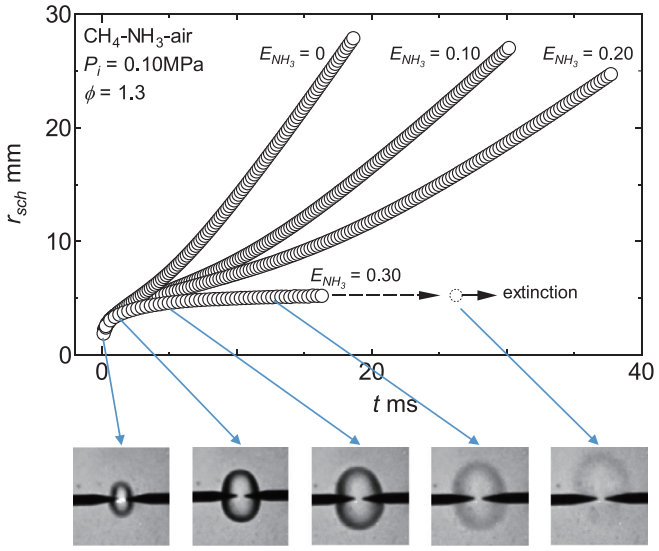

Fig. 4. Evolution of the flame radius with time for the flames at equivalence ratio of 1.3. Images of the flame of $E_{NH_3} = 0.3$ show the propagation sequence of the flame before quenching.

Figure 4 shows the radius-time history of the flames at equivalence ratio of 1.3. At $\phi = 1.3$, the flame of $E_{NH_3} = 0.3$ quenched at a radius of about 5 mm. After ignition, the flame kernel developed and expanded due mainly to the influence of the deposited spark energy. As the spark energy is dissipated, the flame propagation stalled and the image contrast decreased until the flame quenched. Images of the flame showing the propagation sequence before quenching is also shown in Fig. 4. This same observation was recorded after increasing the electrostatic energy charged into the capacitor of the CDI circuit from 0.3 J to 5.5 J. The quenching of the flame could be due to heat losses, stretch and curvature effects. It can be inferred from the following discussions that the flame of $E_{NH_3} = 0.3$ at 1.3 may have the smallest burning velocity and the highest positive sensitivity to stretch of all flames in this study. In other words, the flame may have the lowest rate of heat release from chemical reaction and the highest tendency to quench under the influence of flame stretch.

4.2. Measured laminar burning velocity

Figure 5 shows the variation of the stretched flame speed with the flame stretch rate for some of the flames. With an increase in ammonia concentration and equivalence ratio, the s_n vs. ε relationship changed from linear to non-linear. For the CH_4–air flames ($E_{NH3} = 0$) at lean conditions, s_n varied approximately linearly with ε. On the other hand, the flames with high ammonia concentration at rich conditions such as the flame of $E_{NH3} = 0.2$ at $\phi = 1.3$,

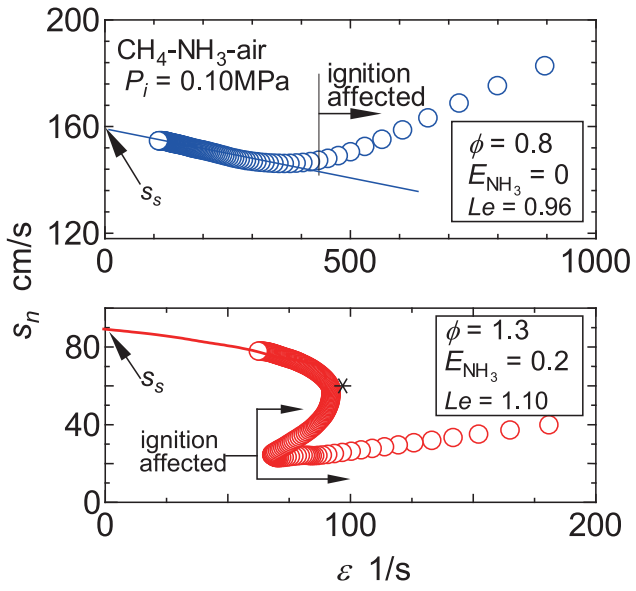

Fig. 5. Variation of the stretched flame speed with flame stretch rate showing a linear and a non-linear s_n vs. ε relationships for two different mixtures with Lewis numbers close to unity.

exhibited a non-linear s_n vs. ε relationship as shown in Fig. 5. This change from a linear to a non-linear s_n vs. ε relationship as ϕ and E_{NH_3} increased was due to an increase in the response of the flame to stretch owing mainly to the influence of the flame thickness as discussed in Section 4.6.

Note that the Z shape of the s_n vs. ε curve for the rich flame is due to the influences of radiative heat losses, thermo-diffusive effects and the external energy input from the spark, all of which control the propagation trajectory of the spherical flame. Theoretical studies have shown that when the flame is initiated without any external energy input, the trajectory includes only the middle and upper branches of the curve. In that case, the flame may start with zero flame speed and stretch rate (flame ball solution) and transit into a propagating spherical flame. A rapid increase in flame speed after flame initiation results to an increase in flame stretch rate in spite of the simultaneous increase in flame radius. This can be seen in Fig. 6 for the flame of $E_{NH3} = 0.2$ at $\phi = 1.3$. The lower branch is introduced when the flame is initiated by an external energy input such as a spark and the spark energy may influence the trajectory up to and slightly beyond the adiabatic extinction limit (indicated by asterisk) depending on the magnitude of the deposited energy [41,42].

The unstretched laminar burning velocity was extracted using Eqs. (4) and (5). To avoid the influence of the ignition energy on

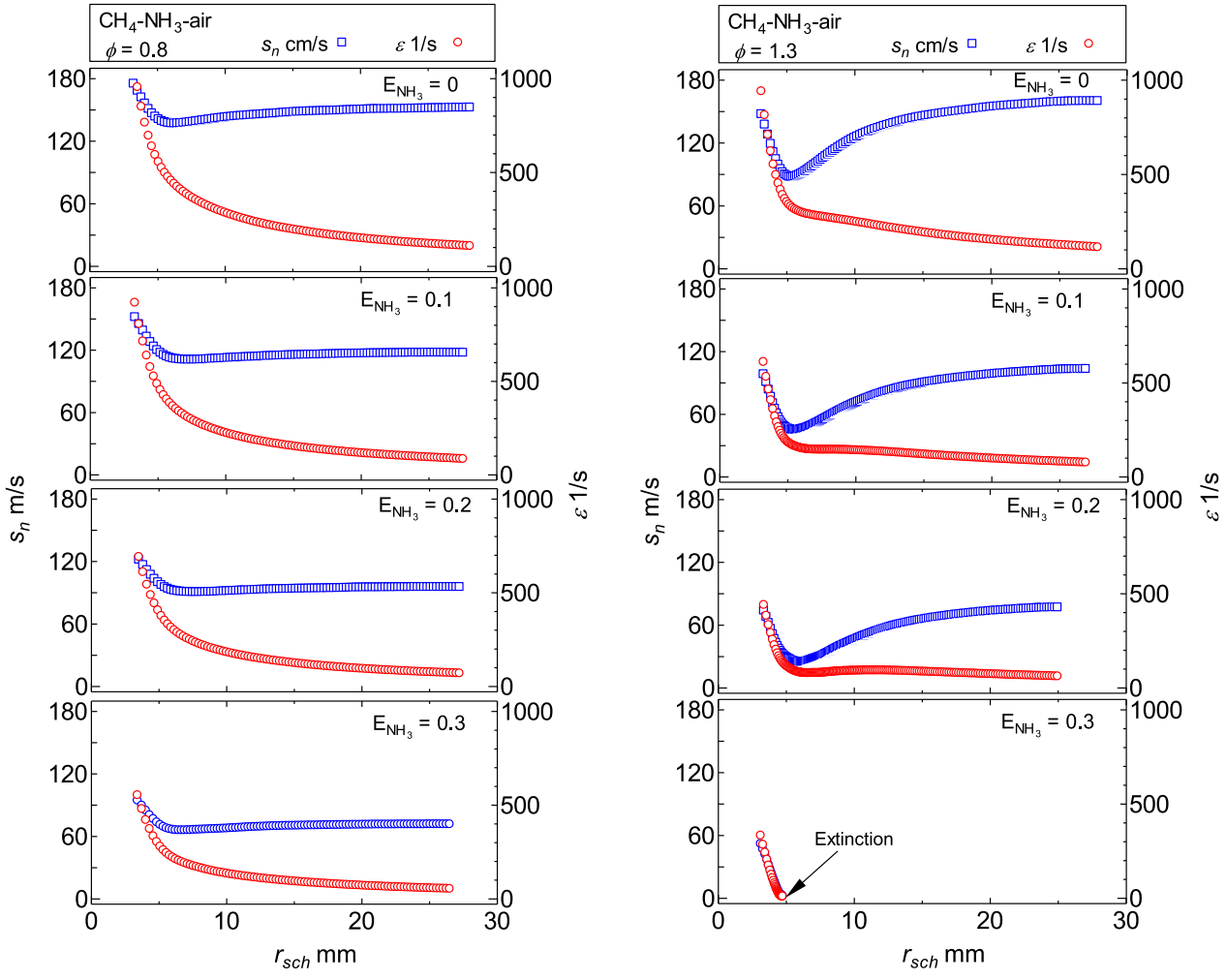

(a) $\phi = 0.8$ (b) $\phi = 1.3$

Fig. 6. Flame speed and total stretch rate as functions of flame radius for the flames at equivalence ratios of (a) 0.8 and (b) 1.3.

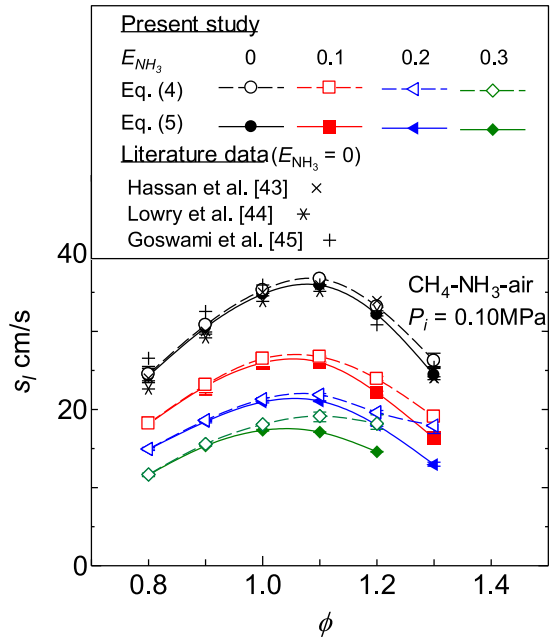

Fig. 7. Comparison of the unstretched laminar burning velocity obtained from the linear and the non-linear correlations.

the measured unstretched laminar burning velocity, flame radii of not less than 10 mm were used for the extrapolations. The range of radius used for the extrapolations was about 15 mm. As shown in Fig. 7, the disparity in the measured values of s_l from the two extrapolation equations increased as ϕ and E_{NH_3} increased. As the relationship between s_n and ε became increasingly non-linear, the linear stretch extrapolation resulted in increasingly inaccurate larger values of s_l. The increasing disparity in the two results corresponds with the increasing sensitivity of the flames to stretch as discussed in Section 4.6. Figure 7 also shows a good agreement of s_l from the present study with literature data [42–45] for pure methane–air flames.

4.3. Comparison of results from the experiments and numerical simulations

Figure 8 shows the measured unstretched laminar burning velocity plotted along with the results of one-dimensional simulations using Tian Mech [25], Mendiara Mech [29], GRI Mech 3.0 [19], UCS mechanism [21] and the present model, developed based in GRI Mech 3.0 [19] and Tian Mech [25]. The error bars are a measure of the uncertainty in the measurements as discussed previously. The effects of radiation, which results to a decrease in the burning velocity of a non-adiabatic flame from that of an adiabatic one, was calculated using the fuel-independent correlation in [46]. As shown, Tian Mech [25] significantly underestimates the measured unstretched laminar burning velocity. The accuracy of the mechanism seems to improve with an increase in ammonia concentration, i.e. with a decrease in the methane content in the fuel. Tian Mech [25] was developed and validated with measured species concentration in stoichiometric methane–ammonia–air flames with varying ammonia concentration in the fuel from 0 (pure methane) to 50% volume fraction at 4 kPa. As discussed in the next section, the HCO→CO conversion path may result to a significant under prediction of the unstretched laminar burning velocity of methane–air flames by Tian Mech [25] at 0.10 MPa. Mendiara Mech [29] was developed based on Tian Mech [25] with special focus on the direct interaction between nitrogen containing radicals and CO_2 and between hydrocarbons and amine species and it consists of 97 species and 779 reactions. Mendiara Mech [29] overpredicts the measured unstretched laminar burning velocity. The UCS Mech [21] is a combination of the hydrocarbon and the nitrogen mechanisms by University College at San Diego and consists of

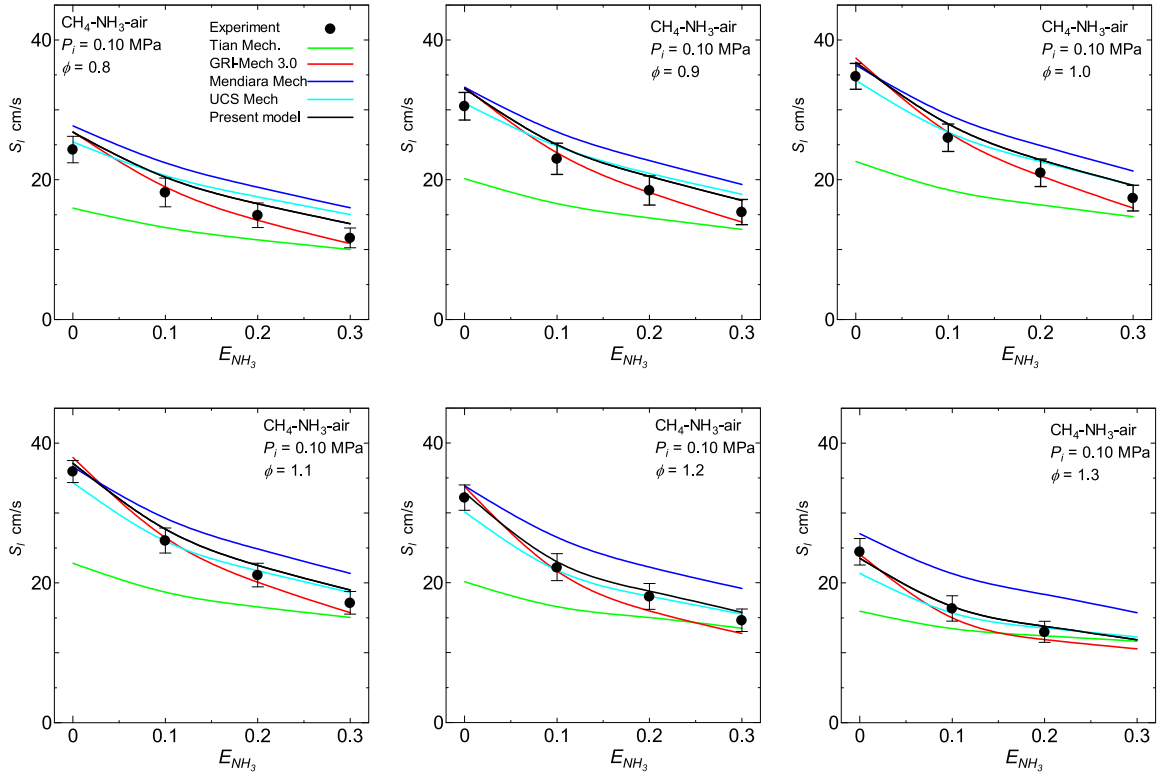

Fig. 8. Comparison of the measured unstretched laminar burning velocity with the simulated values.

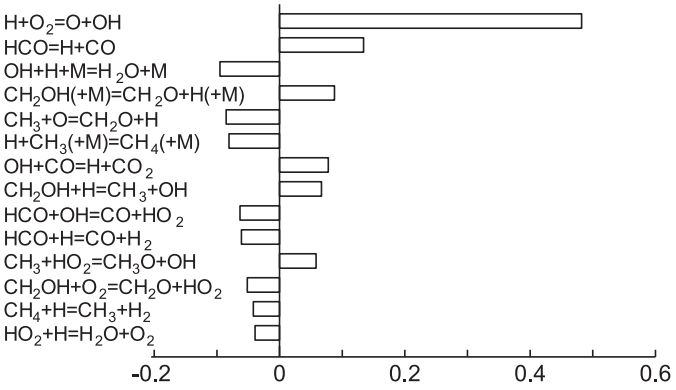

Fig. 9. Normalised sensitivity coefficient of the unstretched laminar burning velocity of stoichiometric CH_4–air flame based on Tian Mech [25] at 0.10 MPa.

65 species and 300 elementary reactions. UCS Mech [21] does not model the measured burning velocity satisfactorily. GRI Mech 3.0 [19] and the present model replicate the unstretched laminar burning velocity satisfactorily, although GRI Mech 3.0 [19] may predict a faster decrease in s_l with E_{NH3}. As discussed in the next section, GRI Mech 3.0 [19] does not contain some important NH_3 oxidation steps relevant in flames with high NH_3 content.

4.4. Methane–ammonia flames chemistry

Tian Mech [25] has been shown by Hayakawa et al. [7] to model the burning velocity of ammonia–air flames the most satisfactorily in comparison with the mechanisms by Miller et al. [22], Lindstedt et al. [23], and Konnov [24]. Furthermore, in comparison with GRI Mech 3.0 [19], Mendiara Mech [29] and Konnov's mechanism [24], Tian Mech [25] has been reported to most satisfactorily predict NO_x emission from a gas turbine combustor fuelled with a mixture of methane and ammonia with 61% ammonia volume fraction [47]. However, Fig. 8 shows that Tian Mech [25] largely underestimates the burning velocity of the flames with $E_{NH3} < 0.3$. First order normalised sensitivity of the burning velocity of stoichiometric methane–air flames to the rate constants of the elementary reactions computed using Tian Mech [25] is shown in Fig 9. Since Tian Mech [25] models the burning velocity of ammonia–air and ammonia–hydrogen–air flames better than most ammonia kinetic mechanisms even at elevated pressures [7,11], the reason for the large underestimation of the burning velocity of methane flames by the mechanism at 0.10 MPa may be due to the carbon-specific rate-limiting reactions. It was found that the large underestimation is due to the influence of the HCO→CO conversion steps shown in Fig. 9. Formyl radical conversion to CO proceeds through the direct decomposition reaction;

$$HCO = CO + H \quad (R1)$$

and the H atom transfer reactions;

$$HCO\ (+H,\ OH,\ O_2) = CO\ (+H_2,\ H_2O,\ HO_2). \quad (R2,\ R3,\ R4)$$

Figure 9 shows that (R1) has the second strongest positive influence on the burning velocity of methane flames while (R2) and (R3) have significant negative influences. The direct decomposition reaction, (R1) facilitates H radical production and promotes the propagation of chain reactions, while the H atom transfer reactions have a chain terminating character. The competition between these two sets of reactions has a significant effect on H radical production and may determine much of the overall behaviour of the methane combustion mechanism [48]. Studies in literature show that the temperature sensitive (R1) is the dominant path for formyl radical consumption in the flame, therefore the net effect of HCO→CO conversion is the facilitation of H radical production and promotion of the chain branching reactions [48–50]. This dominance of (R1) in HCO→CO conversion in the flame chemistry is modeled in GRI Mech 3.0 [19], UCS Mech [21] and ARAMCO mechanism [20]. However, in Tian Mech [25] at 0.10 MPa, (R1) is dominated by (R2, R3, R4), which account for about 80% of formyl radical conversion to CO. In other words, the HCO→CO path in Tian Mech [25] acts as a consumption path for OH and H radicals at 0.10 MPa, consequently facilitating the termination of the chain reactions. It was found that at 4 kPa at which Tian Mech [25] was validated, (R1) is the dominant conversion step for HCO→CO in the flame. However, the unimolecular (R1) in Tian Mech [25] is not as pressure sensitive as the bimolecular (R2), (R3), and (R4), hence the bimolecular reactions dominate (R1) in the conversion of HCO→CO when the pressure increases to 0.10 MPa. It is also worth noting that by updating the rate constants of (R1) using data from Ref. [51] thereby making (R1) the dominant HCO→CO conversion step at 0.10 MPa, Tian Mech [25] satisfactorily modelled the unstretched laminar burning velocity of methane–air flames at 0.10 MPa.

On the other hand, GRI Mech 3.0 [19], is a widely used reaction mechanism for modelling natural gas combustion, developed through validation and optimisation against a large number of experimental targets and includes NO formation and reduction chemistry. It has been well validated with measured values of the laminar burning velocity of methane–air flames and methane–air flames with trace quantities of ammonia [26]. However, GRI Mech 3.0 [19] does not include some important ammonia oxidation mechanism which are important for mixtures with significant ammonia concentration such as the flames of $E_{NH3} \geq 0.1$ in this study. Reactions of the type $NH_i + NH_j = \text{products}$ (i, $j = 0$, 1, 2) and their subsequent products are not included in GRI Mech 3.0 [19]. These reactions do not play an important role in situations where NH_3 is available only in trace quantities in the fuel. However, they are very relevant reactions steps in ammonia flames and in flames of mixtures with significant ammonia concentration, especially at rich conditions. Furthermore, the NO reduction steps (R5) and (R6) are not included in GRI Mech 3.0 [19].

$$NO + NH_2 = N_2 + H_2O \quad (R5)$$

$$NO + NH_2 = NNH + OH \quad (R6)$$

Reactions (R5) and (R6) are the key to the Thermal De-NO_x mechanism (selective non-catalytic reduction of NO) in ammonia flame chemistry [27]. Again, these NO re-burn reactions are not relevant in flames with only trace quantities of ammonia, however their absence may lead to large over prediction of NO emission from flames with significant ammonia concentration as discussed in Section 4.5. GRI Mech 3.0 [19] has been reported to largely over predict measured NO_x emission from a gas turbine burner fuelled with methane–ammonia mixtures with 61% volume fraction of ammonia in the fuel [47].

For accurate modelling of flame stabilisation and NO emissions from gas turbine combustors fired with the methane–ammonia fuels, a reaction mechanism that not only models the burning velocity of the flames satisfactorily but also satisfactorily predicts emissions from the flames is needed. For that purpose, the present model which consists of 59 species and 356 elementary reactions, was developed based on the complete carbon chemistry of GRI Mech 3.0 [19], with the addition of some important NH_3 chemistry of Tian Mech [25]. The high precision rate constant of the chain branching reaction (R7) reported by Hong et al. [52] was adopted

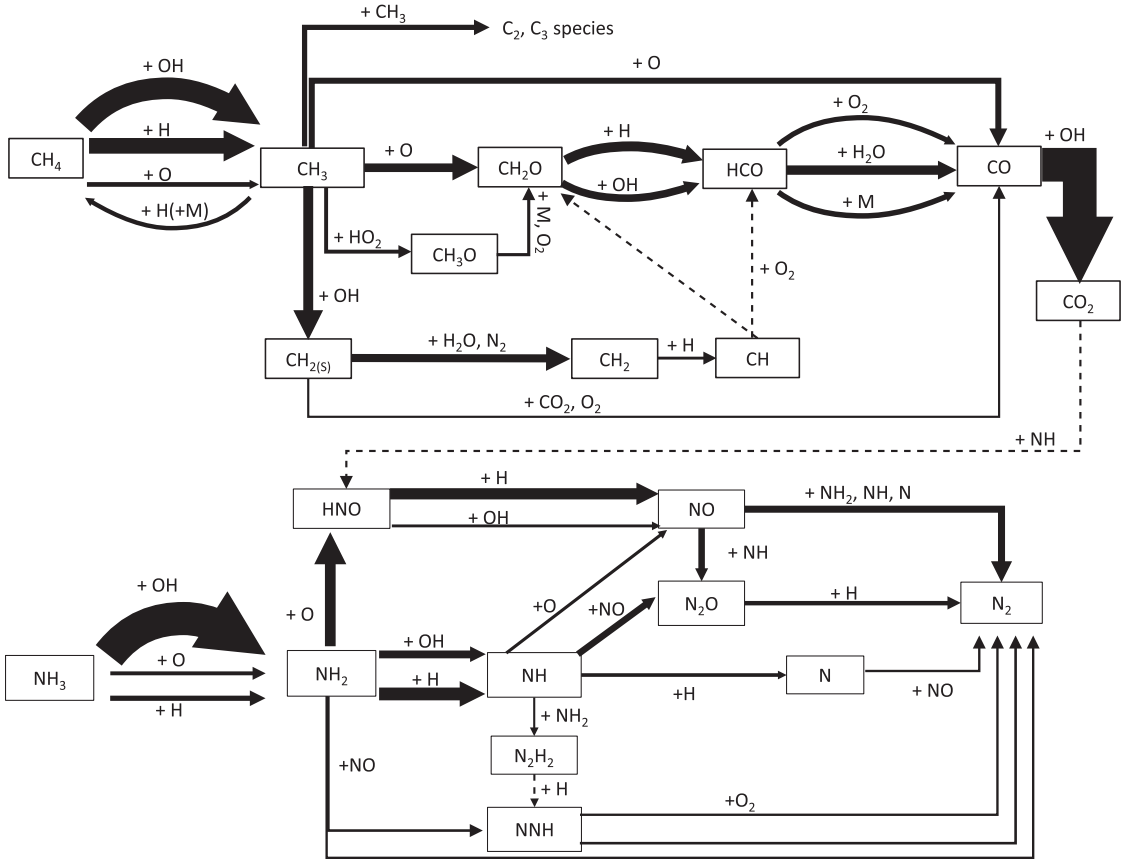

Fig. 10. Reaction path of stoichiometric methane-ammonia-air of $E_{NH_3} = 0.3$ computed using the present model.

in the model. The model is provided as supplementary data to this present study.

$$H + O_2 = OH + O \quad (R7)$$

Figure 10 shows the reaction path of stoichiometric methane–ammonia–air flame of $E_{NH_3} = 0.3$ computed using the present model. The thickness of the arrows corresponds to the relative rate of production (RROP) of species by each path, which was defined as the integrated rate of species production from a chemical step or set of chemical steps normalised by the integrated rate of species production from the reaction $CH_4 + OH = CH_3 + H_2O$. The integration was done over the entire width of the computation domain. Represented in the figure with solid lines are reaction steps with RROP of not less than 0.1. The steps represented by dotted lines have RROP less than 0.1 but was included for completeness or to show links between the methane oxidation chemistry and the ammonia oxidation chemistry. There is no significant direct interaction between the methane oxidation path and ammonia oxidation path, which may affect the burning velocity of the mixtures. The methane chemistry and the ammonia chemistry indirectly interact though their dependence on the same H, OH and O radical pool. With ammonia addition to methane, the H abstraction reactions of methane, methyl radical, ammonia, and amine radicals compete for these radicals. The availability of these radicals facilitates the consumption of the fuels and propagation of the chain branching reactions, which speeds up the overall reaction rate. The reactions from ammonia chemistry with the most influence on the H and OH radical concentration in methane–ammonia chemistry include (R6), (R8) and (R9).

$$NH_2 + O = HNO + H \quad (R8)$$

$$HNO + H = NO + H_2 \quad (R9)$$

The forward step of (R6) has a positive influence on the concentration of the radicals while those of (R8) and (R9) exert negative influence on the radical pool. Although (R8) produces H radicals, it is the predominant HNO production path in the flame. The produced HNO promotes high rate of H radical consumption through (R9). Figure 11 shows that (R6), (R8) and (R9) are the most important rate-limiting reactions from ammonia chemistry in methane–ammonia flames. These reactions have significant control on the burning velocity of the ammonia containing mixtures and their control on the burning velocity increase with ammonia concentration as shown in Fig. 11. However, (R8) exerts less negative influence on the burning velocity of ammonia–air flames because even though it is the predominant HNO production step in ammonia flames [29], HNO consumption through (R9) and (R10) have significant negative and positive effects, respectively on the radical pool.

$$H + NO + M = HNO + M \quad (R10)$$

Therefore, the impact of ammonia chemistry on the burning velocity of methane–ammonia flames is mainly through the influence on the H and OH radicals' concentration in the flame. A decrease in the radical pool with ammonia concentration may slow down the overall reaction rate and, consequently, result in a decrease in the flame speed.

As the mixtures get richer, reactions between amine radicals and their subsequent products become increasingly prominent in methane—ammonia flames, and so does their influence on the burning velocity. $N_2H_3 + H = N_2H_2 + H_2$ and $N_2H_2 + H = NNH +$

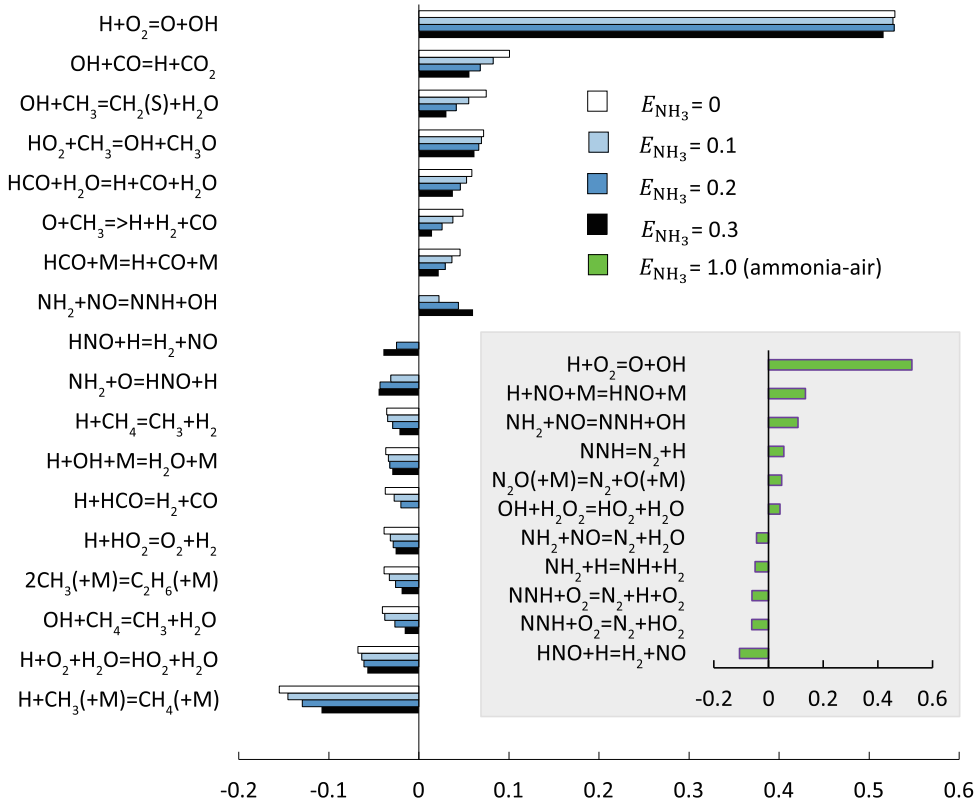

Fig. 11. Normalised first order sensitivity of the unstretched laminar burning velocity with respect to the rate constants of the most rate-limiting reactions in stoichiometric methane–ammonia–air flames. The insert is that for ammonia–air flames.

H_2 were found to have appreciable influence on the unstretched laminar burning velocity at equivalence ratios of 1.2 and 1.3.

4.5. Comparison of present model with other detailed kinetics models

The profiles of temperature, CH_4, NH_3, CO, CO_2, H_2, and NO of the stoichiometric flames of $E_{NH3} = 0$ and 0.3 computed using GRI Mech 3.0 [19], Tian Mech [25] and the present model are compared in Fig. 12. The temperature and species profiles of methane–air flames computed using the present model agree satisfactorily with ones computed using GRI-Mech 3.0 [19]. The ammonia oxidation steps included in the present model has no significant effects on the profiles of premixed methane–air flames. For the flame of $E_{NH_3} = 0.30$, however, the present model predicts significantly lower NO concentration in the flame than GRI Mech 3.0 [19] does, thus agreeing more closely with the results obtained using Tian Mech [25]. Note that the suitability of Tian Mech [25] over GRI Mech 3.0 [19] in predicting NO_x emission from methane–ammonia flames with high ammonia concentration has been reported [47].

Figure 13 shows the variation of NO concentration at the right boundary of the computation domain (10 cm from the origin) with equivalence ratio for the flames of $E_{NH3} = 0$ and 0.3. For the methane–air flame, $E_{NH3} = 0$, the present model agrees with GRI Mech 3.0 [19] for all equivalence ratios while Tian Mech [25] predicts appreciably lower values of NO concentration for at rich conditions. On the other hand, for the flame of $E_{NH3} = 0.3$ the present model agrees with Tian Mech [25] at all equivalence ratios while GRI Mech 3.0 [19] predicts higher concentration of NO especially at lean conditions.

NO reduction in the stoichiometric methane–ammonia flame proceeds mainly through the reaction of NO with NH_i (where $i = 0$, 1, 2) and $NO + NH_2$ reactions, (R5) and (R6), constitute the second largest NO consumption path as shown in Fig. 10. As Fig. 14 shows, the $NH_2 + NO$ reactions are among the most important reactions controlling NO concentration in the flames of the mixtures with ammonia content. Miller et al. [27] noted that the direct or indirect regeneration of OH and O radicals by $NH_2 + NO = NNH + OH$ sustains the Thermal De-NO_x mechanism in ammonia chemistry. It was found that the relative importance of these reactions to NO reduction in methane–ammonia flames increase with a decrease in equivalence ratio. It is thus considered that the absence of these important NO reduction path in GRI Mech 3.0 [19] may contribute to the over prediction of NO concentration in methane-ammonia flames, especially at lean conditions.

4.6. Markstein length

The sensitivity of the laminar burning velocity to flame stretch rate was evaluated by measuring the burned gas Markstein length, L_b. Figure 15 shows values of L_b obtained in this study using Eq. (5). The burned gas Markstein length increased with equivalence ratio and ammonia concentration. Data reported by Chen [39] for methane–air flames are also shown on the figure for comparison with present result.

Asymptotic analysis of the premixed flame structure have shown that L_b is related to the Lewis number, *Le*, the Zel'dovich number, *Ze*, the preheating zone thickness, δ_l and thermal expansion coefficient, σ as follows [34].

$$L_b = \delta_l[f_1(\sigma) + Ze(Le - 1)f_2(\sigma)] \tag{6}$$

where $f_1(\sigma)$ and $f_2(\sigma)$ are functions of σ which are always positive for realistic values of σ. In this study, the Lewis number and the thermal expansion coefficient did not vary significantly with ammonia concentration. The increase in the burned gas Markstein length with ammonia concentration may be due to the influ-

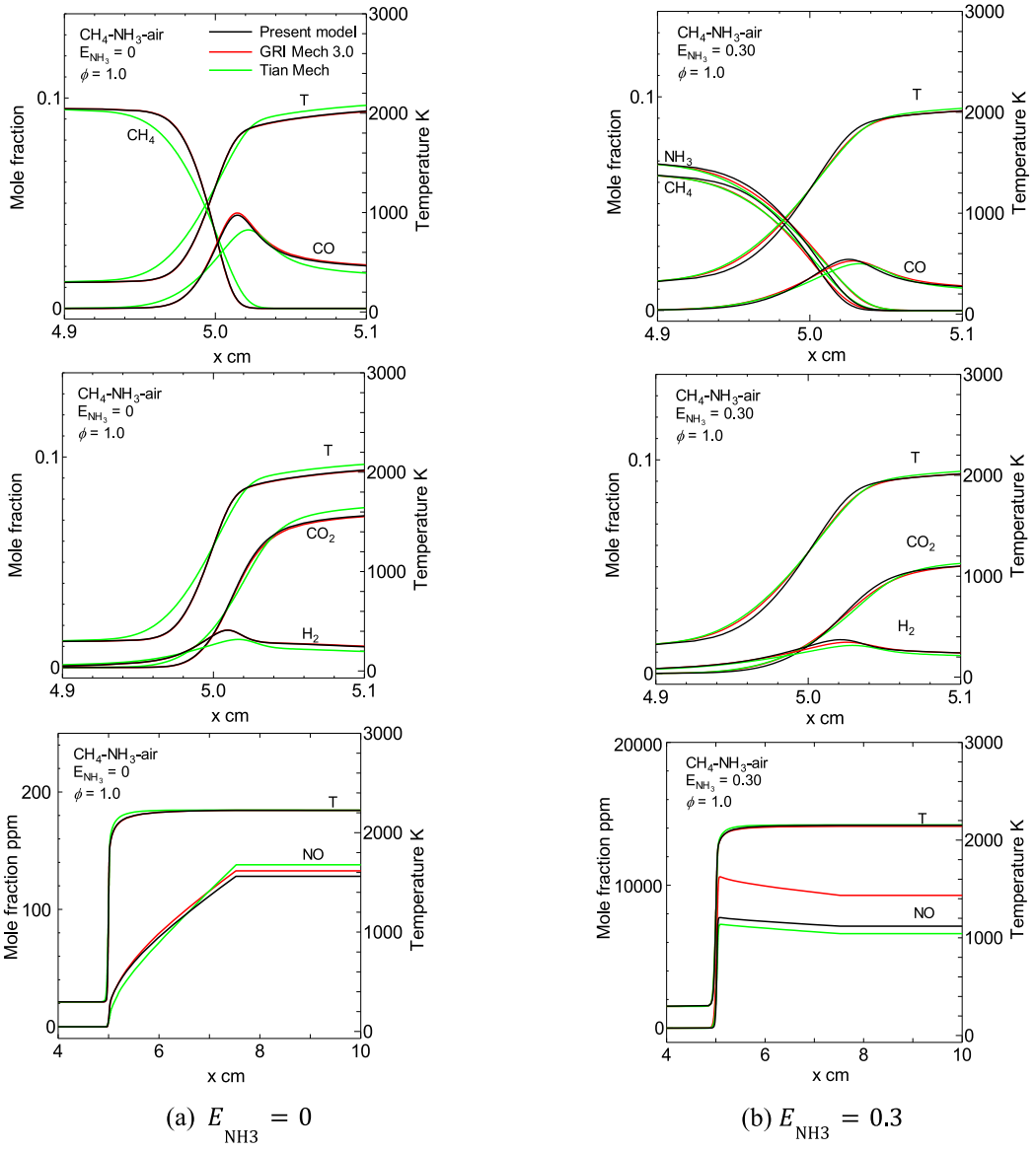

Fig. 12. Profiles of temperature, CH_4, NH_3, CO, CO_2, H_2 and NO of the stoichiometric flames of $E_{NH3} = 0$ and 0.3.

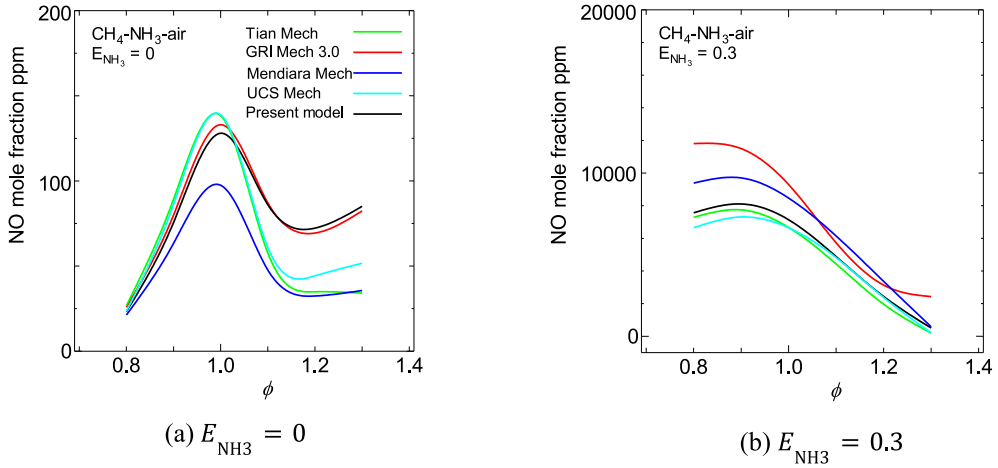

Fig. 13. Variation of NO concentration at the right boundary of the computation domain (10 cm from the origin) with equivalence ratio for the flames of (a) $E_{NH3} = 0$ and (b) $E_{NH3} = 0.3$.

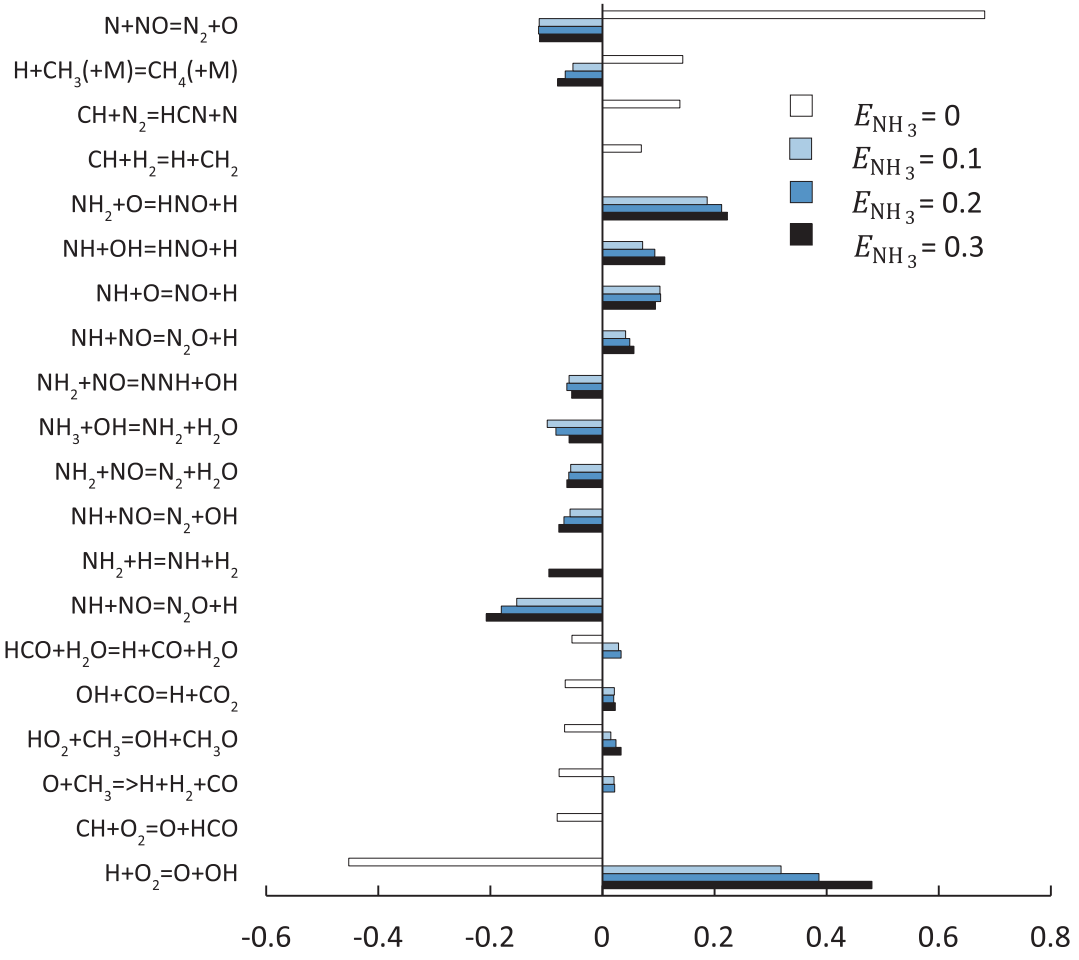

Fig. 14. First order normalised sensitivity of NO concentration to the rate constants of the elementary reactions at the point of maximum NO concentration in the flame. The figure presents the most important elementary reactions in the flames.

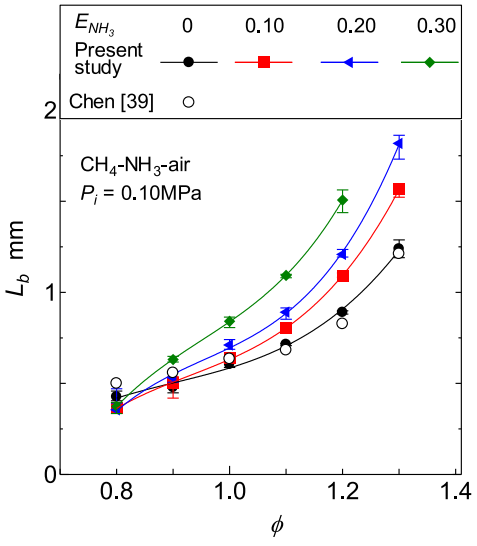

Fig. 15. Variation of the Markstein length with the equivalence ratio and ammonia concentration in the binary fuel.

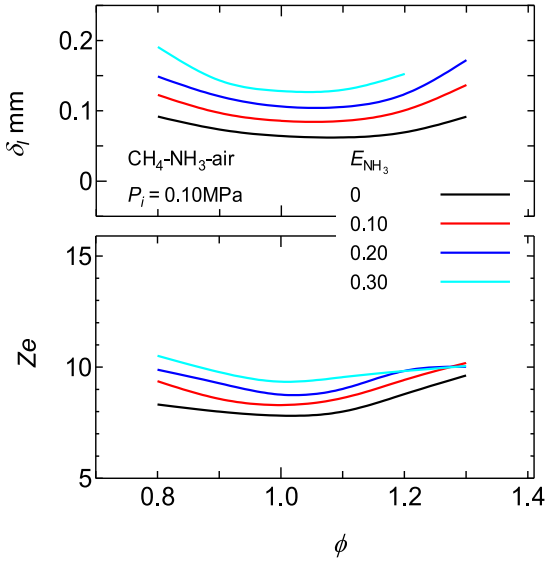

Fig. 16. Variations of the preheating zone thickness and the Zel'dovich number with the equivalence ratio and ammonia concentration in the binary fuel.

ence of the preheating zone thickness and the Zel'dovich number. Figure 16 is plots of δ_l and Ze at different conditions. The preheating zone thickness was given by $\delta_l = \lambda/(\rho_u c_p s_l)$; where λ and c_p are the thermal conductivity of the mixture and specific heat of the mixture at constant pressure, respectively. The preheating zone thickness increased with ammonia concentration in the fuel. Note that the effect of curvature on the laminar burning velocity increases with an increase in the flame thickness [53], thus L_b may

increase with an increase in the preheating zone thickness as suggested by Eq. (6). On the other hand, the Zel'dovich number which may express the sensitivity of the laminar burning velocity to variations in the maximum flame temperature was obtained from the temperature profile of the flames [18]. As shown in Fig. 15, *Ze* increased with an increase in ammonia concentration in the fuel. Because *Ze* promotes the effects of a non-unity Lewis number, the effect of an increase in *Ze* on the sensitivity of the flames to stretch depends on the value of the Lewis number. The increase in the *Ze* may contribute to an increase in L_b for the rich flames in this study which have $Le > 1$. On the other hand, the increase in *Ze* tends to result to a decrease in L_b for the lean flames. The burned gas Markstein lengths of the lean flames increased with ammonia concentration, except at $\phi = 0.8$, because the influence of the preheating zone thickness may be more dominant than that of the Zel'dovich number [54].

5. Conclusions

The unstretched laminar burning velocity of methane–ammonia–air mixtures was studied experimentally using a constant volume chamber and numerically using detailed reaction mechanisms at 298 K and 0.10 MPa over a range of equivalence ratios and ammonia concentration, defined based on the mole-weighted heat fraction of ammonia in the fuel. Analysis of the flame chemistry was also conducted and a detailed chemical kinetic was developed based on GRI Mech 3.0 [19] and Tian Mech [25] to model the laminar burning velocity and NO concentration in the flames. The burned gas Markstein length of the flames was also measured in the experiments. The results in this study are summarised as follows;

1. The unstretched laminar burning velocity of the mixtures decreased non-linearly with an increase in the ammonia concentration. The data from the present study agree with the available literature data on methane–air flames.
2. Tian Mech [25], Mendiara Mech [29], and UCS Mech [21] do not satisfactorily reproduce the burning velocity of the mixtures. The large under prediction of the burning velocity but Tian Mech [25] was found to be mainly due to the dominance of HCO $(+\mathrm{H}, \mathrm{OH}, \mathrm{O_2}) = \mathrm{CO} (+\mathrm{H_2}, \mathrm{H_2O}, \mathrm{HO_2})$ over $\mathrm{HCO} = \mathrm{CO} + \mathrm{H}$ in the conversion of HCO to CO. GRI Mech 3.0 [19] predicts the measured unstretched laminar burning velocity closely, although it does not contain some important reactions in ammonia combustion chemistry. The present model predicts the laminar burning velocity satisfactorily.
3. The predominant rate-limiting reactions in methane–ammonia flames, which belong to the ammonia oxidation path were found to be $\mathrm{NO} + \mathrm{NH_2} = \mathrm{NNH} + \mathrm{OH}$, $\mathrm{NH_2} + \mathrm{O} = \mathrm{HNO} + \mathrm{H}$ and $\mathrm{HNO} + \mathrm{H} = \mathrm{NO} + \mathrm{H_2}$. Of all other elementary reactions in ammonia oxidation path, these three reactions have the most significant control on the H and OH radicals' concentration in methane–ammonia flames. Therefore, the impact of ammonia chemistry on the burning velocity of methane–ammonia flames is mainly through the influence on the H and OH radicals' concentration.
4. Temperature and species profiles of methane–air flames computed with the present model agree with those computed using GRI Mech 3.0. For the flames with high ammonia content, the NO concentration predicted by the present model agrees with that of Tian Mech [25]. The absence of $\mathrm{NH_2} + \mathrm{NO} = \mathrm{NNH} + \mathrm{OH}$ and $\mathrm{NH_2} + \mathrm{NO} = \mathrm{N_2} + \mathrm{H_2O}$ in GRI Mech 3.0 [19] may contribute to over prediction of NO concentration in methane–ammonia flames with substantial ammonia content.
5. The sensitivity of the flame to stretch increased with equivalence ratio and ammonia concentration, as indicated by the increase in the burned gas Markstein length, leading to a shift from a linear to a non-linear flame speed-stretch rate relationship as the equivalence ratio and ammonia concentration increased. The increase in the burned gas Markstein length with ammonia concentration was found to be mainly due to an increase in the preheating zone thickness. Hence, non-linear flame speed-stretch behaviour may occur in flames with Lewis numbers close to unity if the flame thickness is large enough.

Acknowledgements

This research was supported by the Council for Science, Technology and Innovation (CSTI), the Cross-ministerial Strategic Innovation Promotion Program(SIP), "Energy Carriers" (Funding Agency: the Japan Science and Technology Agency (JST)).

Supplementary materials

Supplementary material associated with this article can be found, in the online version, at doi:10.1016/j.combustflame.2017.09.002.

References

[1] K. Goshome, T. Yamada, H. Miyaoka, T. Ichikawa, Y. Kojima, High compressed hydrogen production via direct electrolysis of liquid ammonia, Int. J. Hydrogen Energy 41 (2016) 14529–14534.
[2] C. Zamfirescu, I. Dincer, Ammonia as a green fuel and hydrogen source for vehicular applications, Fuel Process. Technol. 90 (2009) 729–737.
[3] R. Michalsky, B.J. Parman, V. Amanor-Boadu, P.H. Pfromm, Solar thermochemical production of ammonia from water, air and sunlight: thermodynamic and economic analyses, Energy 42 (2012) 251–260.
[4] S.J. Yang, H. Jung, T. Kim, C.R. Park, Recent advances in hydrogen storage technologies based on nanoporous carbon materials, Prog. Nat. Sci. 22 (2012) 631–638.
[5] J.T. Gray, E. Dimitroff, N.T. Meckel, R.D. Quillian Jr., Ammonia fuel–engine compatibility and combustion, SAE paper 660156 (1966). doi:10.4271/660156.
[6] F.J. Verkamp, M.C. Hardin, J.R. Williams, Ammonia combustion properties and performance in gas-turbine burners, Symp. (Int.) Combust. 11 (1967) 985–992.
[7] A. Hayakawa, T. Goto, R. Mimoto, Y. Arakawa, T. Kudo, H. Kobayashi, Laminar burning velocity and Markstein length of ammonia/air premixed flames at various pressures, Fuel 159 (2015) 98–106.
[8] O. Kurata, N. Iki, T. Matsunuma, T. Inoue, T. Tsujimura, H. Furutani, H. Kobayashi, A. Hayakawa, Performances and emission characteristics of NH_3–air and NH_3–CH_4–air combustion gas-turbine power generations, Proc. Combust. Inst. 36 (2017) 3351–3359.
[9] P. Kumar, T.R. Meyer, Experimental and modeling study of chemical-kinetics mechanisms for H 2-NH3-air mixtures in laminar premixed jet flames, Fuel 108 (2013) 166–176.
[10] J. Li, H. Huang, N. Kobayashi, Z. He, Y. Nagai, Study on using hydrogen and ammonia as fuels: combustion characteristics and NO_x formation, Int. J. Energy Res. 38 (2014) 1214–1223.
[11] A. Ichikawa, A. Hayakawa, Y. Kitagawa, K.D.K.A. Somarathne, T. Kudo, H. Kobayashi, Laminar burning velocity and Markstein length of ammonia/hydrogen/air premixed flames at elevated pressures, Int. J. Hydrogen Energy 40 (2015) 9570–9678.
[12] A. Valera-Medina, S. Morris, J. Runyon, D.G. Pugh, R. Marsh, P. Beasley, T. Hughes, Ammonia, methane and hydrogen for gas turbines, Energy Procedia. 75 (2015) 118–123.
[13] A.J. Reiter, S.C. Kong, Combustion and emissions characteristics of compression-ignition engine using dual ammonia-diesel fuel, Fuel 90 (2011) 87–97.
[14] A.J. Reiter, S.C. Kong, Demonstration of compression-ignition engine combustion using ammonia in reducing greenhouse gas emissions, Energy Fuels 22 (2008) 2963–2971.
[15] F.N. Egolfopoulos, N. Hansen, Y. Ju, K. Kohse-Höinghaus, C.K. Law, F. Qi, Advances and challenges in laminar flame experiments and implications for combustion chemistry, Prog. Energy Combust. Sci. 43 (2014) 36–67.
[16] D. Bradley, M. Lawes, M.S. Mansour, Correlation of turbulent burning velocities of ethanol–air, measured in a fan-stirred bomb up to 1.2MPa, Combust. Flame 158 (2011) 123–138.
[17] D. Bradley, A.K.U. Lau, M. Lawes, Flames stretch rate as a determinant of turbulent burning velocity, Phil. Trans. R. Soc. Lond. Ser. A 338 (1992) 359–387.
[18] E.C. Okafor, Y. Nagano, T. Kitagawa, Experimental and theoretical analysis of cellular instability in lean H_2-CH_4-air flames at elevated pressures, Int. J. Hydrogen Energy 41 (2016) 6581–6592.
[19] G.P. Smith, D.M. Golden, M. Frenklach, N.W. Moriarty, B. Eiteneer, M. Goldenberg, et al., GRI Mech 3.0. Gas Research Institute, available at <http://www.me.berkeley.edu/gri_mech/>.

[20] W.K. Metcalfe, S.M. Burke, S.S. Ahmed, H.J. Curran, A hierarchical and comparative kinetic modeling study of C1–C2 hydrocarbon and oxygenated fuels, Int. J. Chem. Kinet. 45 (2013) 638–675.
[21] , University of California at San Diego, 2011 http://web.eng.ucsd.edu/mae/groups/combustion/mechanism.html.
[22] J.A. Miller, M.D. Smooke, R.M. Green, R.J. Kee, Kinetic modelling of the oxidation of ammonia in flames, Combust. Sci. Technol. 34 (1983) 149–176.
[23] R.P. Lindstedt, F.C. Lockwood, M.A. Selim, Detailed kinetic modelling of chemistry and temperature effects on ammonia oxidation, Combust. Sci. Technol. 99 (1994) 253–276.
[24] A.A. Konnov, Implementation of the NCN pathway of prompt-NO formation in the detailed reaction mechanism, Combust. Flame 156 (2009) 2093–2105.
[25] Z. Tian, Y. Li, L. Zhang, P. Glarborg, F. Qi, An experimental and kinetic modelling study of premixed $NH_3/CH_4/O_2$/Ar flames at low pressure, Combust. Flame 156 (2009) 1413–1426.
[26] P.F. Henshaw, T. D'Andrea, K.R.C. Mann, D.S.-K. TING, Premixed ammonia-methane-air combustion, Combust. Sci. Technol. 177 (2005) 2151–2170.
[27] J.A. Miller, C.T. Bowman, Mechanism and modelling of nitrogen chemistry in combustion, Prog. Energy Combust. Sci. 15 (1989) 287–338.
[28] Ø. Skreiberg, P. Kilpinen, P. Glarborg, Ammonia chemistry below 1400K under fuel-rich conditions in a flow reactor, Combust. Flame 136 (2004) 501–518.
[29] T. Mendiara, P. Glarborg, Ammonia chemistry in oxy-fuel combustion of methane, Combust. Flame 156 (2009) 1937–1949.
[30] Z. Chen, On the accuracy of laminar flame speeds measured from outwardly propagating spherical flames: methane/air at normal temperature and pressure, Combust. Flame 162 (2015) 2442–2453.
[31] P.D. Ronney, H.Y. Wachman, Effect of gravity on laminar premixed gas combustion I: flammability limits and burning velocities, Combust. Flame 62 (1985) 107–119.
[32] CHEMKIN-PRO 17.2, ANSYS, Inc.: San Diego, (2016).
[33] D. Bradley, P.H. Gaskell, X.J. Gu, Burning velocities, Markstein lengths, and flame quenching for spherical methane-air flames: a computational study, Combust. Flame 104 (1996) 176–198.
[34] P. Clavin, Dynamic behaviour of premixed flame fronts in laminar and turbulent flows, Prog. Energy Combust. Sci. 11 (1985) 1–59.
[35] E. Hu, Z. Huang, J. He, H. Miao, Experimental and numerical study on laminar burning velocities and flame instabilities of hydrogen-air mixtures at elevated pressures and temperatures, Int. J. Hydrogen Energy 34 (2009) 8741–8755.
[36] D. Bradley, R.A. Hicks, M. Lawes, C.G.W. Sheppard, R. Woolley, The measurement of laminar burning velocities and Markstein numbers for iso-octane–air and iso-octane–n- heptane–air mixtures at elevated temperatures and pressures in an explosion bomb, Combust. Flame 115 (1998) 126–144.
[37] C.K. Law, O.C. Kwon, Effects of hydrocarbon substitution on atmospheric hydrogen-air flame propagation, Int. J. Hydrogen Energy 29 (2004) 867–879.
[38] A.P. Kelley, C.K. Law, Nonlinear effects in the extraction of laminar flame speeds from expanding spherical flames, Combust. Flame 156 (2009) 1844–1851.
[39] Z. Chen, On the extraction of laminar flame speed and Markstein length from outwardly propagating spherical flames, Combust. Flame 158 (2011) 291–300.
[40] F. Wu, W. Liang, Z. Chen, Y. Ju, C.K. Law, Uncertainty in stretch extrapolation of laminar flame speed from expanding spherical flames, Proc. Combust. Inst. 35 (2015) 663–670.
[41] Z. Chen, Y. Ju, Theoretical analysis of the evolution from ignition kernel to flame ball and planar flame, Combust. Theory Modell. 11 (2007) 427–453.
[42] Z. Chen, M.P. Burke, Y. Ju, Effects of Lewis number and ignition energy on the determination of laminar flame speed using propagating spherical flames, Proc. Combust. Inst. 32 (2009) 1253–1260.
[43] M.I. Hassan, K.T. Aung, G.M. Faeth, Measured and predicted properties of laminar premixed methane/air flames at various pressures, Combust. Flame 115 (1998) 539–550.
[44] W. Lowry, J. de Vries, M. Krejci, E. Petersen, Z. Serinyel, W. Metcalfe, H. Curran, G. Bourque, Laminar flame speed measurements and modeling of pure alkanes and alkane blends at elevated pressures, J. Eng. Gas Turbines Power 133 (2011) 91501.
[45] M. Goswami, S.C.R. Derks, K. Coumans, W.J. Slikker, M.H. de Andrade Oliveira, R.J.M. Bastiaans, C.C.M. Luijten, L.P.H. de Goey, A.A. Konnov, The effect of elevated pressures on the laminar burning velocity of methane+air mixtures, Combust. Flame 160 (2013) 1627–1635.
[46] H. Yu, W. Han, J. Santner, X. Gou, C.H. Sohn, Y. Ju, Z. Chen, Radiation-induced uncertainty in laminar flame speed measured from propagating spherical flames, Combust. Flame 161 (2014) 2815–2824.
[47] H. Xiao, A. Valera-Medina, R. Marsh, P.J. Bowen, Numerical study assessing various ammonia/methane reaction models for use under gas turbine conditions, Fuel 196 (2017) 344–351.
[48] C.K. Westbrook, F.L. Dryer, Chemical kinetic modeling of hydrocarbon combustion, Prog. Energy Combust. Sci. 10 (1984) 1–57.
[49] R.S. Timonen, E. Ratajczak, D. Gutman, A.F. Wagner, The addition and dissociation reaction $H + CO = HCO$. 2. Experimental studies and comparison with theory, J. Phys. Chem. 91 (1987) 5325–5332.
[50] S. Hochgreb, F.L. Dryer, A comprehensive study on CH_2O oxidation kinetics, Combust. Flame 91 (1992) 257–284.
[51] C.L. Rasmussen, J.G. Jakobsen, P. Glarborg, Experimental measurements and kinetic modeling of CH_4/O_2 and $CH_4/C_2H_6/O_2$ conversion at high pressure, Int. J. Chem. Kinet. 41 (2008) 498–506.
[52] Z. Hong, D.F. Davidson, E.A. Barbour, R.K. Hanson, A new shock tube study of the $H + O2 = OH + O$ reaction rate using tunable diode laser absorption of H_2O near 2.5 mm, Proc. Combust. Inst. 33 (2011) 309–316.
[53] O.C. Kwon, G. Rozenchan, C.K. Law, Cellular instabilities and self-acceleration of outwardly propagating spherical flames, Proc. Combust. Inst. 29 (2002) 1775–1783.
[54] P. Kelley, J. Smallbone, D.L. Zhu, C.K. Law, Laminar flame speeds of C5 to C8 n-alkanes at elevated pressures: experimental determination, fuel similarity, and stretch sensitivity, Proc. Combust. Inst. 33 (2011) 963–970.